Nanoscale

Accepted Manuscript

This article can be cited before page numbers have been issued, to do this please use: I. M. Bjørge, I. S. Choi, C. R. Correia and J. Mano, *Nanoscale*, 2019, DOI: 10.1039/C9NR06267J.

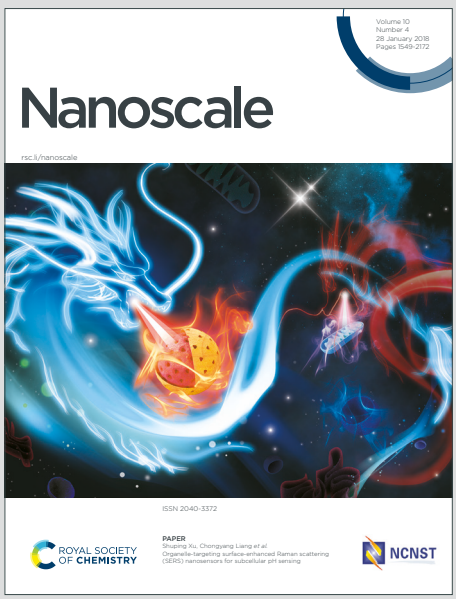

ROYAL SOCIETY OF CHEMISTRY

rsc.li/nanoscale

View Article Online
DOI: 10.1039/C9NR06267J

COMMUNICATION

Nanogrooved microdiscs for bottom-up modulation of osteogenic differentiation

Received 00th January 20xx,
Accepted 00th January 20xx

DOI: 10.1039/x0xx00000x

Isabel M. Bjørge,[a] Insung S. Choi, [b] Clara R. Correia,[a†] and João F. Mano [a†]

Grooved topographical features have effectively modulated cell differentiation on two-dimensional substrates. To transpose patterning into a 3D context, nanogrooved microdiscs, "topodiscs", are produced as cell-carriers for bottom-up cell-mediated assembly. While enhancing cell proliferation, topodiscs led to the formation of bone-like aggregates, even in culture medium lacking osteoinductive factors.

Introduction

At a nanometric scale, bone is mostly composed of hydroxyapatite reinforced collagen molecules.[1] Mineralized collagen molecules are arranged parallelly to form collagen fibrils, which, in turn, are also arranged parallelly to form fibers.[2] Understanding and taking advantage of bone physiology appears as an option to inspire bone tissue engineering strategies.[3] Both at a nano and micrometric level, the organization of the extracellular matrix (ECM) is a preponderant factor in cell-matrix signaling.[4,5] Topographical features deliver mechanical signals to cells, which are converted intracellularly into biochemical signals.[6] In order to take advantage of such mechanotransduction mechanisms, tailoring surface topography has gained momentum and several studies have explored the influence of ridges/grooves,[7] pillars,[8,9] bead monolayers,[10] and holes.[11] When cells are seeded on microgrooves, contact guidance directs cell alignment, growth, and migration along the microgroove direction.[12,13]

Furthermore, surface topography can actively guide the differentiation fate of mesenchymal stem cells (MSCs) into osteogenic or adipogenic lineages by directing cells to become elongated or rounded, respectively.[7,14] This effect has been linked to the mechanotransduction of surface cues. When cell spreading is stimulated, larger focal adhesions are formed and a greater actin- myosin contractility is observed, linked to an increased intracellular tension and transfer of tensile forces to the nucleus, which may in fact impact chromosomal arrangement. Conversely, when MSCs are seeded on substrates that restrict spreading, the rounded cell morphology impedes the formation of mature adhesions, consequently directing adipogenic differentiation.[15] Similarly, MSCs seeded on nanoholes or nanopillars are more likely to differentiate and form hyaline cartilage than when seeded on nanoridges in the same nanometric range.[11] In turn, myoblast fusion into multinucleated myotubes is enhanced when seeded on grooves, even in the absence of differentiation medium.[16] Additionally, grooved substrates with different nano and microgroove/ridge widths have been shown to direct the differentiation pathway of stem cells towards osteogenic,[17] myogenic,[18] neuronal,[19] and chondrogenic lineages.[11]

The osteogenic potential of grooved substrates has thus been previously established, however available studies are limited to a 2D approach, which does not mimic the native environment of cells.[12,20,21] Bottom-up approaches are an attractive option for the development of 3D constructs for tissue engineering as they rely on the assembly of smaller units that can be implanted through minimally invasive procedures.[22] Microparticles support cell expansion and form 3D robust structures through cell-microparticle aggregation, which can be injected independently or encapsulated.[23–25]

Hence, we developed flat microparticles with topographical features, specifically grooves, here termed as topodiscs, that allow to transpose topographical cues to a 3D cell culture environment. This new class of microparticles features (1) disc-like shape with enhanced surface/volume ratio to maximize cell-adhesion sites; and (2) grooved patterning on the surface to control cell orientation or adhesion and direct osteogenic differentiation. Through a bottom-up cell-mediated approach, cells interact with topodiscs via not only ventral but also dorsal receptors, allowing for a three-dimensional cell stimulation. Topodiscs thus act as cell carriers, supporting cell expansion and adhesion, while also delivering topographical cues via surface patterning to direct osteogenic differentiation, even in the absence of osteogenic factors.

[a] CICECO – Aveiro Institute of Materials, Department of Chemistry, University of Aveiro, Campus Universitário de Santiago, 3810-193 Aveiro, Portugal.
[b] Korea Adv Inst Sci & Technol, Dept Chem, Ctr Cell Encapsulat Res, Daejeon 34141, South Korea
† Corresponding authors.
Electronic Supplementary Information (ESI) available: [details of any supplementary information available should be included here]. See DOI: 10.1039/x0xx00000x

Results and discussion

μsphere and topodisc characterization

Grooved substrates have been previously shown to impact cell alignment and differentiation into the osteogenic lineage, where pitch dimensions (groove plus ridge dimensions) ranging from 400 nm [17] to 200 μm [26] have been assessed. Furthermore, it has been demonstrated that grooved substrates tend to enhance osteogenic differentiation to a greater extent than flat substrates.[7,18,20,26–28] These studies have however been restricted to a two-dimensional approach, which does not fully mimic the native environment of cells. The present study aims to transpose the reaction of cells to patterning to a quasi-3D concept, as topodiscs were applied for a bottom-up cell-mediated assembly to form three-dimensional constructs.

CDs were used as grooved substrates, presenting ridge widths of 1185±16 nm, groove widths of 412±12 nm, and ridge heights of 197±14 nm. Initially, counter-molds of CDs were prepared using water-soluble poly(vinyl alcohol) (PVA). As can be observed in Figure 1A, PVA counter-molds presented a homogeneously patterned surface, maintaining the fidelity of CD surfaces (Figure S1). Upon molding of polycaprolactone (PCL) microparticles (μspheres), the obtained topodiscs were collected and visualized by SEM. Topodiscs were successfully produced and presented the homogenous grooved patterning of the mold (Figure 1A). The shape of topodiscs is elongated due to the preferential flow of PCL from the microparticles along the ridges of the mold during the processing. Topodiscs presented an average length of 92±20 μm and width of 55±19 μm (Figure 1B), with patterning dimensions of 944±49 nm ridges, 358±23 nm grooves, and 201±45 nm ridge height. Furthermore, topodiscs presented on average the quadruple of the surface area comparatively to μspheres. The large standard deviation observed for all measured and calculated parameters is due to the variance in size of the initial template used – μpsheres, which were sieved to be comprised between 25 and 40 μm. Of note, topodiscs allowed the adhesion of cells, which aligned along the microgrooves of the topodisc, as showed in Figure 1A.

Topodiscs as cell carriers for pre-osteoblastic MC3T3-E1 cell line

Topodiscs were then studied for their ability to perform as cell carriers, comparatively to μspheres. As a proof-of-concept, a MC3T3-E1 pre-osteoblastic cell line was used. Figure 2A shows that both substrates supported cell adhesion. Additionally, cells' ability to proliferate was demonstrated since only small aggregates could be visualized on day 1, and larger cell-mediated aggregates were formed up to day 21. Spherical microparticles have been previously used as vehicles for cell proliferation via bottom-up approaches to form 3D constructs on their own [23] or when encapsulated.[29] Hence, it was expected that both μspheres and topodiscs would sustain cell culture, as was observed.

Upon 21 days of culture, the deposition of extracellular matrix (ECM) on the exterior of aggregates is evident for both types of substrates (Figure 2B). In cross-section images it is possible to observe cells bridging several microparticles. Cells can attach to more than one μsphere or topodisc, promoting the cohesion of cell-particle assembly. Hence, cells interact in both cases with particles via ventral and dorsal receptors, allowing for a complete cell stimulation, contrarily to what would occur in a 2D environment. The construction of aggregates is controlled by cells, which selectively remodel particle location, while depositing extracellular matrix. Whereas there is only a 3D aggregation of μspheres mediated by cells, for topodiscs there is both a 3D aggregation and alignment of cells along surface microgrooves. The surface area of topodiscs is sufficiently large for the adherence of several cells, yet topodisc dimensions still allow for cell-mediated remodeling. Furthermore, higher magnification of formed aggregates allows to observe that the morphology of the ECM deposited on topodiscs and μspheres is quite distinct. Interestingly, a very fibrillar and highly aligned ECM was deposited on topodiscs, whereas a more compact ECM was deposited on μspheres, even if also seemingly aligned. During the 21-day assays, cells were allowed to interact freely with topodiscs and form randomly-shaped aggregates. The bottom-up assembly of microparticles has been previously established and pose as attractive options for minimally invasive injectable applications due to their ability to assemble *in situ*.[23,30] In order to demonstrate the potential of topodiscs for these same applications, cells and topodiscs were seeded at a higher density on hydrophilic spots engraved on superhydrophobic slides with varying shapes [31] and, upon a day in culture, it was verified that cell-topodisc aggregates acquired the different shapes, namely squares, circles, and hexagons (Figure S2).

In order to compare both types of microparticles as vehicles for cell culture, cell metabolic activity and cell proliferation was assessed. A significant difference in both metabolic activity and cell proliferation of MC3T3-E1 cells was observed between topodiscs and μspheres (Figure 2C and D). Topodiscs clearly led to an increased cell expansion in both basal and osteogenic medium, likely due to the larger surface area to volume ratio for cells to proliferate.

Topodiscs as osteogenic-inducing platforms in the absence of osteoinductive factors

In order to determine the osteogenic potential of topodiscs versus commonly used μspheres, mineralization upon 21 days in culture was assessed. To this end, hASCs were cultured in the presence (OST) or absence (BAS) of osteogenic factors. Histological cuts of hASC aggregates were stained with Masson's Trichrome and Von Kossa to specifically mark collagen (blue) and phosphate deposits (black), respectively. Hydroxyapatite (green) present in aggregates was specifically stained to further confirm mineralization (Figure 3).

In regard to collagen deposition, a greater staining was observed for cells cultured with topodiscs, even in the absence of osteogenic factors, than for μsphere aggregates (Figure 3). Collagen presence in μsphere aggregates in basal medium was nearly negligible and even in osteogenic medium was quite reduced when compared with topodiscs. Collagen is a prime

component of bone, with 85 to 90% of the total bone protein consisting of collagen fibers.[1] Cell interaction with a collagen-containing ECM is also a requirement for the stimulation of osteogenic differentiation.[32] Hence, the enhanced collagen staining of topodisc aggregates, even without osteogenic factors, is an important indicator of commitment to the osteogenic lineage. In accordance, a previous study featuring 50 and 200 µm grooves composed of compacted osteogenic factor-loaded microspheres presented a significantly increased collagen secretion than flat substrates.[33] However, in the absence of osteogenic factors, collagen content and osteogenic quantifiers (ALP and osteocalcin) were only significantly enhanced on 50 µm grooves relatively to flat substrates and presented much lower results when compared to osteogenic factor-loaded substrates.[33]

To assess tissue mineralization, the presence of phosphate deposits and hydroxyapatite was evaluated (Figure 3). By Von Kossa staining, it was possible to observe that a similar phosphate deposition occurred in topodisc aggregates in both basal and osteogenic medium, as for µspheres in osteogenic medium. Virtually no phosphate deposits were observed for µsphere aggregates in the absence of osteogenic factors. A similar trend was observed for hydroxyapatite staining where topodisc aggregates clearly presented a greater hydroxyapatite content. Furthermore, a comparable amount of hydroxyapatite appeared to be present in cell-topodisc aggregates in both basal and osteogenic medium. Cell-µsphere aggregates required osteogenic factors to induce formation of hydroxyapatite, even if slightly reduced when compared with topodiscs, and no hydroxyapatite staining was found in samples cultured in basal medium. Hence, it can be concluded that a mineralized matrix was effectively achieved. Considering both the enhanced collagen deposition and matrix mineralization, the osteogenic potential of topodiscs alone, without the need for osteogenic factors, as platforms for osteogenic differentiation was demonstrated.

Previous studies have been limited to a 2D approach, reporting that grooved patterning can effectively direct cell alignment and enhance osteogenic differentiation to a greater extent than flat surfaces.[7,26,27] The enhancement of osteogenic differentiation has also been shown to be cell-dependent, where optimal conditions may in fact be associated with maximal cell length, highlighting the effect of contact guidance and tensile stress on differentiation.[20,34] Kim *et al.* demonstrated that 0.5/1.8, 2/2, and 2/4 µm ridges/grooves, in the presence of osteogenic factors, induced osteogenic differentiation with a greater alizarin red staining observed for MC3T3-E1 cells seeded on 0.5/1.8 µm (500 nm depth) substrates, whereas hASCs presented an enhanced staining on 2/2 and 2/4 µm (1 µm depth) substrates. Additionally, half-doses of osteogenic supplements on hASCs grown on 2/2 µm substrates were comparable to full-doses.[20] In accordance with these findings and also in the presence of osteogenic factors, Abagnale *et al.* [7] observed a greater alizarin red staining of hASCs on 2 µm ridges, than for other ridge widths studied up to 15 µm, somewhat independently of groove width, which was also varied between 2 and 15 µm. Watari *et al.* [17] demonstrated that human bone marrow-derived mesenchymal stem cells (hBMSCs) cultured on 200/200 nm ridges/grooves presented an enhanced calcium deposition and expression of osteogenic marker genes RUNX2 and BGLAP comparatively with non-patterned substrates in the absence of osteoinductive factors, yet a combination of topography with osteogenic factors yielded the best results. Ridge/groove widths of 700/700 nm and 2/2 µm were also studied yet did not present as promising results as 200 nm grooves, even if BGLAP expression was significantly higher than for flat surfaces. Ridge depth may also be an impacting factor for the differences observed between these studies as 1 or 2 µm depths were used by Kim *et al.* [20] and Abagnale *et al.*,[7] respectively, as opposed to 300 nm by Watari *et al.*[17] Hence, even though the 2D effect of patterning had previously been established, the effect in a 3D environment, which mimics the native environment in a more realistic manner, had yet to be proved.

In this study, ridge/groove dimensions present on topodiscs were approximately 944/358 nm, with 201 nm in depth. In accordance with 2D studies, hASC differentiation into the osteogenic lineage was effectively enhanced by the patterned surface of topodiscs, when compared with smooth-surface µspheres.[7,26,27] It is complicated to reach a consensus regarding the optimal dimensions for patterned surfaces due to the fact that ridges and grooves can be tailored at a nanometric scale, opening up an infinitude of possibilities. Despite this fact, patterning dimensions in this study could to some extent be correlated with dimensions applied in previously mentioned studies. Hence, the enhancement of osteogenic potential due to the topographical features present on the surface of topodiscs is further corroborated. More importantly, a similar enhancement of osteogenic differentiation for cells cultured on patterned topodiscs in the absence or presence of osteogenic factors was observed. In previous studies, osteoinductive factors were required for osteogenic differentiation or for comparative results.[7,17,20] We previously used microspheres as cell carriers and showed their *in vitro* bioperformance using a co-culture of microvascular endothelial cells and hASCs. The cellular crosstalk led to the osteogenic differentiation of hASCs in the absence of two major osteogenic differentiation factors, namely dexamethasone and ascorbic acid. However, mineralization could only occur in the presence of β-glycerophosphate.[24] In this work, the proposed topodiscs allowed for a full osteogenic differentiation in the absence of osteoinductive factors, orchestrated by the patterned and three-dimensional environment offered to stem cells by the new engineered topodiscs. This opens up new potential applications, namely for *in vivo* studies, where an initial *in vitro* stimulation prior to implantation with osteoinductive factors may in fact be bypassed and still result in new localized mineralized bone tissue.

Conclusions

Topodiscs featuring nanogrooved patterning were produced for a bottom-up assembly of 3D cell-mediated micro-bone tissues. Topodiscs enabled cell adhesion and led to an enhanced proliferation comparatively with microspheres, likely due to the increased surface area to volume ratio. More importantly and in line with what is observed for 2D patterned substrates, topodiscs effectively led to the osteogenic differentiation of hASCs, even in the absence of osteoinductive factors. The formation of a three-dimensional tissue, which is more mimetic of the native cell environment, may in fact have contributed to the enhanced osteogenic effect. Patterned topodiscs were thus presented as novel cell carriers with nanotopographical cues for osteogenic differentiation, transposing the previously documented 2D osteogenic effect into a 3D setting, while bypassing the need for the osteogenic supplements. With tissue engineering strategies striving to reduce the complexity of systems and minimize the need for additional factors, the osteogenic potential of topodiscs was shown to be dependent on the grooved topographical surface cues. Although, the present work focused on osteogenic differentiation, we envision that the application of these 3D patterned substrates could in fact be broadened to other topography-responsive cells. This technology could thus potentially be used, for example, in neuronal, myogenic, cardiac, or chondrogenic tissue engineering strategies.

Materials and methods

Grooved microdisc (topodisc) production

The production method of topodiscs was performed as illustrated in Scheme 1. Step I: A 5% w/v solution of polycaprolactone (PCL, M_n=80 kDa, Sigma-Aldrich) in dichloromethane (DCM, Honeywell Chemicals) was emulsified under agitation (1:5) with an aqueous 0.5% w/v solution of polyvinyl alcohol (PVA, M_n=30 – 70 kDa, Sigma-Aldrich) for 48 hours to produce PCL microparticles (µpsheres) with a diameter range of 25-40 µm. Step II: Poly(vinyl alcohol) (PVA) counter-molds of optical media substrates (CDs) were produced via solvent evaporation of a 12% w/v solution of PVA in distilled water on CDs at 40ºC. PVA membranes sputtered with gold-palladium were visualized via scanning electron microscopy (SEM, S4100, Hitachi). Step III: µspheres were dispersed in patterned PVA membranes and pre-heated at 75ºC for 25 min prior to imprinting. A second patterned PVA membrane was placed on top of pre-heated µspheres with an applied pressure of approximately 1 kPa for 5 min. Step IV: Upon cooling, PVA-entrapped PCL membranes were dissolved in distilled water under stirring. Step V: Topodiscs were collected by centrifugation and extensively washed in distilled water. Topodiscs and non-molded µspheres were subjected to plasma treatment (Plasma System ATTO, Electronic Diener) at 0.4-0.6 mbar and 30 V for 15 min using atmospheric air, followed by UV sterilization during 30 min.

In vitro cell culture

MC3T3-E1 cells (American Type Culture Collection) were cultured with α-MEM supplemented with 10% fetal bovine serum (FBS, Gibco, ThermoFisher Scientific) and 1% antibiotic-antimycotic (100X, Gibco, ThermoFisher Scientific), denominated basal medium (BAS) at 37ºC in a humidified air atmosphere of 5% CO_2. Cells were detached at 90% of confluence via 0.05% w/v trypsin-EDTA (from porcine pancreas 1:250, Sigma-Aldrich) treatment for 5 min at 37ºC. An identical process was performed with human adipose-derived stem cells (hASCs, passage 4, American Type Culture Collection). A seeding density of $4x10^5$ cells.cm^{-2} was used for MC3T3-E1 cells, whereas $8x10^5$ cells.cm^{-2} was used for hASCs, calculated based on the average surface area of topodiscs. An equal weight of topodiscs and µspheres was used for each condition. Topodisc and µsphere MC3T3-E1-mediated aggregates were cultured in BAS medium, whereas hASC-mediated aggregates were cultured in both BAS and osteogenic (OST) medium supplemented with ascorbic acid (50 µg.mL^{-1}, Cayman Chemical), β-glycerophosphate disodium salt (10 mM, Santa Cruz Biotechnology), and dexamethasone (10 nM, ThermoFisher Scientific).

3D aggregates with controlled shape

Cells were stained with DiL (1,1'-Dioctadecyl-3,3,3',3'-Tetramethylindocarbocyanine Perchlorate (DiIC18(3)), ThermoFisher Scientific) according to the manufacturer's specifications. Stained cells were seeded on previously developed surfaces[31] at a concentration of $5x10^7$ cells.mL^{-1} with 50 mg.mL^{-1} of topodiscs.

Cell-microparticle aggregate characterization

Samples were fixed with 4% v/v formaldehyde solution (Sigma-Aldrich) in PBS for 30 min at RT. For SEM morphological studies, samples were dehydrated in increasing ethanol series for 10 min at RT and sputtering with gold-palladium. For nuclei (blue) and actin filament (red) staining of MC3T3-E1 aggregates, DAPI (4',6-diamidino-2-phenylindole, dihydrochloride, 1 mg.mL^{-1}, ThermoFisher Scientific, 1:1000 ratio in PBS for 5 min, RT) and phalloidin (Flash Phalloidin™ Red 594, 300U, BioLegend, 1:40 ratio in PBS for 45 min, RT) were respectively used, posteriorly to permeabilization with 0.1% v/v Triton-X100 (BioXtra, Sigma-Aldrich) in PBS for 5 minutes. After 21 days in culture of hASC aggregates, hydroxyapatite (green) was stained using OsteoImage mineralization assay kit (Lonza) according to the manufacturer's specifications and counterstained with DAPI as previously described. Histological assessment of hASC aggregates upon 21 days was also performed after fixation in buffered formaldehyde 10% v/v. Samples were processed in an automatic tissue processor (STP120, Microm) and embedded in paraffin. Histological sections (5µm) were cut using a microtome (HM355E, Microm, ThermoFisher Scientific) and stained with Masson's Trichrome and von Kossa for visualization of collagen fibers and phosphate deposits, respectively. Samples were visualized by optical and fluorescence microscopy (Axio Imager 2, Zeiss).

Mitochondrial metabolic activity and cell proliferation quantification

Mitochondrial metabolic activity quantification (n=3) was performed at 1, 7, 14, and 21 days using an MTS colorimetric assay (CellTiter 96 AQueous One Solution Cell Proliferation Assay, Promega) according to the manufacturer's specifications. Absorbance was read at 490 nm using a microplate reader (Synergy HTX, BioTek). Total DNA quantification was performed according to kit specifications (Quant-iTTM PicoGreen® dsDNA assay kit, Life Technologies) after cell lysis in ultra-pure sterile water containing 2% v/v triton-X100. Fluorescence was read at an excitation wavelength of 485/20 nm and emission wavelength of 528/20 nm using a microplate reader.

Statistical analysis

Statistical analysis was performed using two-way analysis of variance (ANOVA) with Tukey's or Sidak's post-hoc test (GraphPad Prism 6.0). A p-value<0.05 was considered statistically significant.

Conflicts of interest

There are no conflicts to declare.

Acknowledgments

I. M. Bjørge acknowledges the Portuguese Foundation for Science and Technology (FCT) with doctoral grant SFRH/BD/129224/2017. This work was financially supported by the European Research Council grant agreement ERC-2014-ADG-669858 (ATLAS) and FCT grant agreement PTDC/BTM-MAT/31064/2017 (CIRCUS). This work was developed within the scope of the project CICECO-Aveiro Institute of Materials, FCT Ref. UID/CTM/50011/2019, financed by national funds through the FCT/MCTES. I. S. Choi acknowledges the Basic Science Research Program through the National Research Foundation of Korea funded by the Ministry of Science, ICT and Future Planning (MSIP 2012R1A3A2026403).

References

1 P. Fratzl, H. S. Gupta, E. P. Paschalis and P. Roschger, *J. Mater. Chem.*, 2004, **14**, 2115–2123.
2 P. Fratzl and R. Weinkamer, *Prog. Mater. Sci.*, 2007, **52**, 1263–1334.
3 D. Lopes, C. Martins-Cruz, M. B. Oliveira and J. F. Mano, *Biomaterials*, 2018, **185**, 240–275.
4 C. J. Bettinger, R. Langer and J. T. Borenstein, *Angew. Chem. Int. Ed. Engl.*, 2009, **48**, 5406–15.
5 E. Lamers, R. van Horssen, J. te Riet, F. C. M. J. M. van Delft, R. Luttge, X. F. Walboomers and J. A. Jansen, *Eur. Cells Mater.*, 2010, **20**, 329–343.
6 S. Dobbenga, L. Fratila-Apachitei and A. A. Zadpoor, *Acta Biomater.*, 2016, **46**, 3–14.
7 G. Abagnale, M. Steger, V. H. Nguyen, N. Hersch, A. Sechi, S. Joussen, B. Denecke, R. Merkel, B. Hoffmann, A. Dreser, U. Schnakenberg, A. Gillner and W. Wagner, *Biomaterials*, 2015, **61**, 316–326.
8 J. Fiedler, B. Özdemir, J. Bartholomä, A. Plettl, R. E. Brenner and P. Ziemann, *Biomaterials*, 2013, **34**, 8851–8859.
9 J. Seo, J. Kim, S. Joo, J. Y. Choi, K. Kang, W. K. Cho and I. S. Choi, *Small*, 2018, **14**, 1801763.
10 K. Kang, S. Y. Yoon, S.-E. Choi, M.-H. Kim, M. Park, Y. Nam, J. S. Lee and I. S. Choi, *Angew. Chemie Int. Ed.*, 2014, **53**, 6075–6079.
11 Y.-N. Wu, J. B. K. Law, A. Y. He, H. Y. Low, J. H. P. Hui, C. T. Lim, Z. Yang and E. H. Lee, *Nanomedicine Nanotechnology, Biol. Med.*, 2014, **10**, 1507–1516.
12 K. Wang, L. Cai, L. Zhang, J. Dong and S. Wang, *Adv. Healthc. Mater.*, 2012, **1**, 292–301.
13 S. Lenhert, M.-B. Meier, U. Meyer, L. Chi and H. P. Wiesmann, *Biomaterials*, 2005, **26**, 563–570.
14 M. Guvendiren and J. A. Burdick, *Biomaterials*, 2010, **31**, 6511–6518.
15 H. Donnelly, M. Salmeron-Sanchez and M. J. Dalby, *J. R. Soc. Interface*, 2018, **15**, 20180388.
16 M. P. Sousa, S. G. Caridade and J. F. Mano, *Adv. Healthc. Mater.*, 2017, **6**, 1601462.
17 S. Watari, K. Hayashi, J. A. Wood, P. Russell, P. F. Nealey, C. J. Murphy and D. C. Genetos, *Biomaterials*, 2012, **33**, 128–136.
18 P.-Y. Wang, W.-T. Li, J. Yu and W.-B. Tsai, *J. Mater. Sci. Mater. Med.*, 2012, **23**, 3015–3028.
19 M. R. Lee, K. W. Kwon, H. Jung, H. N. Kim, K. Y. Suh, K. Kim and K.-S. Kim, *Biomaterials*, 2010, **31**, 4360–4366.
20 C.-S. Kim, J.-H. Kim, B. Kim, Y.-S. Park, H.-K. Kim, H. T. Tran, S. H. Kim, H. Jeon, S. Kim, J. H. Sim, H. M. Shin, G. Kim, Y. J. Baik, K.-J. Lee, H.-Y. Kim, T. J. Yun, Y. S. Kim and H.-R. Kim, *Adv. Funct. Mater.*, 2017, **27**, 1703569.
21 E. Lamers, X. Frank Walboomers, M. Domanski, J. te Riet, F. C. M. J. M. van Delft, R. Luttge, L. A. J. A. Winnubst, H. J. G. E. Gardeniers and J. A. Jansen, *Biomaterials*, 2010, **31**, 3307–3316.
22 J. W. Nichol and A. Khademhosseini, *Soft Matter*, 2009, **5**, 1312–1319.
23 C. A. Custódio, M. T. Cerqueira, A. P. Marques, R. L. Reis and J. F. Mano, *Biomaterials*, 2015, **43**, 23–31.
24 C. R. Correia, R. P. Pirraco, M. T. Cerqueira, A. P. Marques, R. L. Reis and J. F. Mano, *Sci. Rep.*, 2016, **6**, 21883.
25 M. D. Neto, M. B. Oliveira and J. F. Mano, *Trends Biotechnol.*, , DOI:10.1016/j.tibtech.2019.02.008.
26 X. Shi, L. Li, S. Ostrovidov, Y. Shu, A. Khademhosseini and H. Wu, *ACS Appl. Mater. Interfaces*, 2014, **6**, 11915–11923.
27 L. Sun, D. Pereira, Q. Wang, D. B. Barata, R. Truckenmüller, Z. Li, X. Xu and P. Habibovic, *PLoS One*, 2016, **11**, e0161466.
28 K. Matsuzaka, X. F. Walboomers, J. E. de Ruijter and J. A. Jansen, *Biomaterials*, 1999, **20**, 1293–1301.
29 C. R. Correia, P. Sher, R. L. Reis and J. F. Mano, *Soft Matter*, 2013, **9**, 2125–2130.
30 M. B. Oliveira and J. F. Mano, *Biotechnol. Prog.*, 2011, **27**,

897–912.

31 A. I. Neto, K. Demir, A. A. Popova, M. B. Oliveira, J. F. Mano and P. A. Levkin, *Adv. Mater.*, 2016, **28**, 7613–7619.

32 F. Langenbach and J. Handschel, *Stem Cell Res. Ther.*, 2013, **4**, 117.

33 X. Shi, S. Chen, J. Zhou, H. Yu, L. Li and H. Wu, *Adv. Funct. Mater.*, 2012, **22**, 3799–3807.

34 Y. Yang, X. Wang, T.-C. Huang, X. Hu, N. Kawazoe, W.-B. Tsai, Y. Yang and G. Chen, *J. Mater. Chem. B*, 2018, **6**, 5424–5434.

Figures:

Scheme 1. Schematic representation of production method for topodiscs. (I) Polyvinyl alcohol (PVA) counter-molds of CDs were produced by dispensing 12% w/v solution on top of CDs and allowing to dry at 40ºC. (II) PCL particles produced by oil/water emulsion were sieved to obtain [25-40] µm microparticles (µspheres). (III) Subsequently, µspheres were micro-molded between the patterned PVA membranes at an optimized time, temperature, and applied force. (IV) Topodiscs were subjected to several washings to eliminate the PVA counter-mold. (V) Recovery of topodiscs by centrifugation. Topodiscs sustained cell adhesion and proliferation via cell-mediated topodisc aggregation.

Figure 1. µsphere and topodisc characterization. (A) SEM images from left to right of: PVA counter-mold; PCL grooved topodisc with higher magnification of topodisc patterning on border (1) and center (2). (B) µsphere and topodisc dimensions: µsphere diameter (left); topodisc length and width (center); topodisc and µsphere surface area (right).

Figure 2. Pre-osteoblastic MC3T3-E1 culture on topodiscs and µspheres. (A) Fluorescence images of stained F-actin filaments (red) and nuclei (blue) of cells seeded on topodiscs or µspheres at timepoints 1, 7, 14, and 21 days. Cells were seeded at a density of 40 000 cells/cm2, calculated according to the average surface area of topodiscs, and cultured in basal medium. Scale bars correspond to 100 µm. (B) SEM images of cells seeded on topodiscs and µspheres on days 7 and 21 of culture in basal medium. Day 21 images from left to right correspond to cells and topodiscs/µspheres aggregation; cross-sections of respective aggregates with cells; and higher magnification of ECM. (C) SEM images of cells (red) cultured on µspheres or topodiscs, highlighting the 3D cell-mediated aggregation and alignment, for the case of topodiscs, upon 7 days in culture. Control image of cell cultured on a commercially available 2-dimensional polystyrene substrate. (D) Cell metabolic activity determined using an MTS colorimetric assay and (E) cell proliferation determined by DNA quantification. Cells were cultured up to 21 days in basal medium. Mean ± standard deviation for each condition (n=3). All results were significantly different unless marked with ns ($p > 0.05$), indicating no statistically significant differences between samples.

Figure 3. hASCs seeded on topodiscs and µspheres after 21 days of culture in basal (BAS) or osteogenic (OST) medium. Staining of histological cuts with Masson's Trichrome and von Kossa was performed. For Masson's Trichrome, tissue is marked in red and collagen fibers in blue. Von Kossa staining of tissue (blue) and phosphate deposits (black), with arrow exemplifying the identification of deposits. Hydroxyapatite was fluorescently stained in green, whilst cell nuclei were stained in blue (DAPI). Black scale bars correspond to 20 µm, whereas white scale bars correspond to 100 µm.

View Article Online
DOI: 10.1039/C9NR06267J

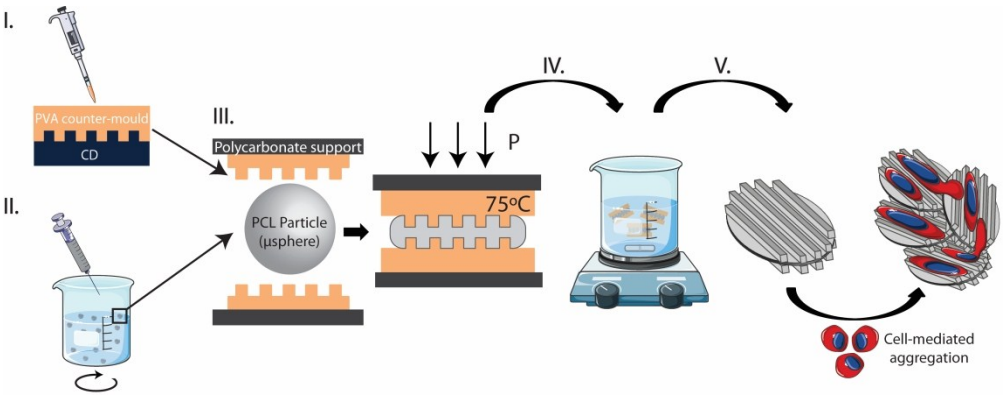

Scheme 1. Schematic representation of production method for topodiscs. (I) Polyvinyl alcohol (PVA) counter-molds of CDs were produced by dispensing 12% w/v solution on top of CDs and allowing to dry at 40ºC. (II) PCL particles produced by oil/water emulsion were sieved to obtain [25-40] μm microparticles (μspheres). (III) Subsequently, μspheres were micro-molded between the patterned PVA membranes at an optimized time, temperature, and applied force. (IV) Topodiscs were subjected to several washings to eliminate the PVA counter-mold. (V) Recovery of topodiscs by centrifugation. Topodiscs sustained cell adhesion and proliferation via cell-mediated topodisc aggregation.

View Article Online
DOI: 10.1039/C9NR06267J

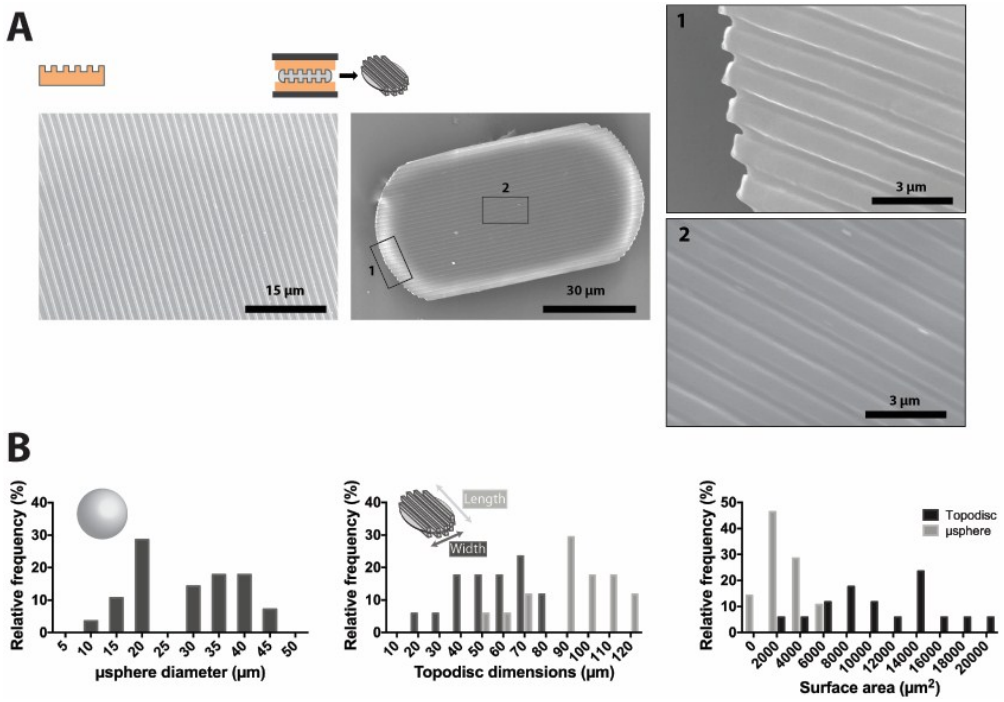

Figure 1. µsphere and topodisc characterization. (A) SEM images from left to right of: PVA counter-mold; PCL grooved topodisc with higher magnification of topodisc patterning on border (1) and center (2). (B) µsphere and topodisc dimensions: µsphere diameter (left); topodisc length and width (center); topodisc and µsphere surface area (right).

View Article Online
DOI: 10.1039/C9NR06267J

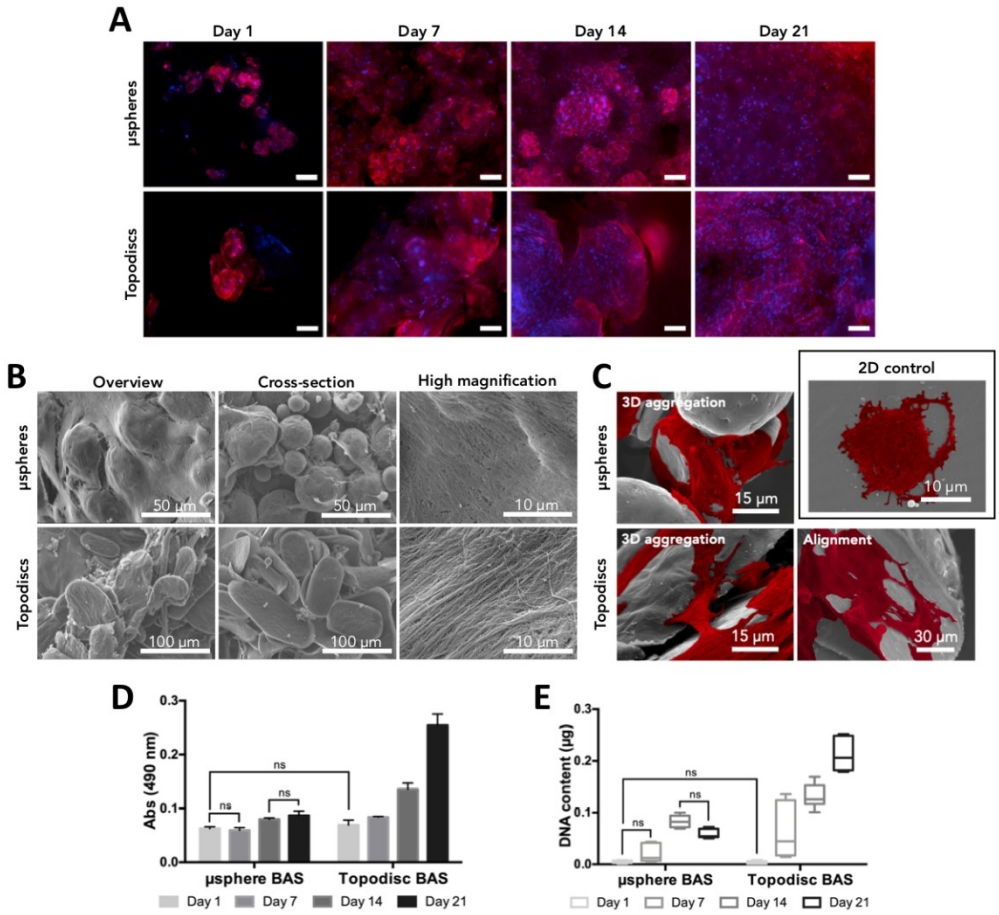

Figure 2. Pre-osteoblastic MC3T3-E1 culture on topodiscs and μspheres. (A) Fluorescence images of stained F-actin filaments (red) and nuclei (blue) of cells seeded on topodiscs or μspheres at timepoints 1, 7, 14, and 21 days. Cells were seeded at a density of 40 000 cells/cm2, calculated according to the average surface area of topodiscs, and cultured in basal medium. Scale bars correspond to 100 μm. (B) SEM images of cells seeded on topodiscs and μspheres on days 7 and 21 of culture in basal medium. Day 21 images from left to right correspond to cells and topodiscs/μspheres aggregation; cross-sections of respective aggregates with cells; and higher magnification of ECM. (C) SEM images of cells (red) cultured on μspheres or topodiscs, highlighting the 3D cell-mediated aggregation and alignment, for the case of topodiscs, upon 7 days in culture. Control image of cell cultured on a commercially available 2-dimensional polystyrene substrate. (D) Cell metabolic activity determined using an MTS colorimetric assay and (E) cell proliferation determined by DNA quantification. Cells were cultured up to 21 days in basal medium. Mean ± standard deviation for each condition (n=3). All results were significantly different unless marked with ns ($p > 0.05$), indicating no statistically significant differences between samples.

202x184mm (150 x 150 DPI)

View Article Online
DOI: 10.1039/C9NR06267J

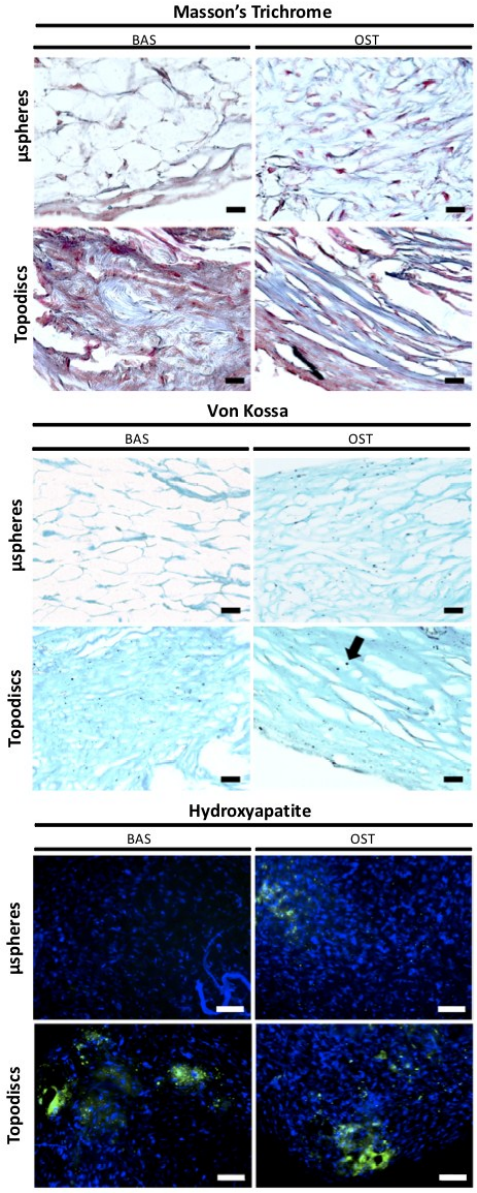

Figure 3. hASCs seeded on topodiscs and µspheres after 21 days of culture in basal (BAS) or osteogenic (OST) medium. Staining of histological cuts with Masson's Trichrome and von Kossa was performed. For Masson's Trichrome, tissue is marked in red and collagen fibers in blue. Von Kossa staining of tissue (blue) and phosphate deposits (black), with arrow exemplifying the identification of deposits. Hydroxyapatite was fluorescently stained in green, whilst cell nuclei were stained in blue (DAPI). Black scale bars correspond to 20 µm, whereas white scale bars correspond to 100 µm.

78x196mm (150 x 150 DPI)

View Article Online
DOI: 10.1039/C9NR06267J

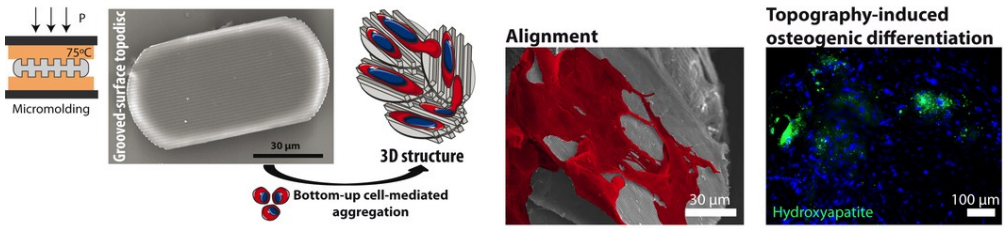

89x20mm (300 x 300 DPI)